Journal of Alloys and Compounds 509 (2011) 8907–8911

Contents lists available at ScienceDirect

Journal of Alloys and Compounds

journal homepage: www.elsevier.com/locate/jallcom

Improving the piezoelectric thermal stability by tailoring phase transition behavior in the new $(1-x)[0.65PbMg_{1/3}Nb_{2/3}O_3–0.35PbTiO_3]–xBiZn_{1/2}Ti_{1/2}O_3$ perovskite solid solutions

Zhenzhu Cao[a,b,c], Guorong Li[b,*], Jiangtao Zeng[b], Siu Wing Or[c,**], Liaoying Zheng[b], Qingrui Yin[b], Lihong Cheng[b]

[a] Chemical Engineering College of Inner Mongolia University of Technology, 49 Aiming Street, Huhehaote 010051, Inner Mongolia, PR China
[b] Key Laboratory of Inorganic Functional Materials and Devices, Shanghai Institute of Ceramics, Chinese Academy of Sciences, 1295 Dingxi Road, Shanghai 200050, PR China
[c] Department of Electrical Engineering, The Hong Kong Polytechnic University, Hung Hom, Kowloon, Hong Kong, China

ARTICLE INFO

Article history:
Received 5 November 2010
Received in revised form 27 May 2011
Accepted 3 June 2011
Available online 1 July 2011

Keywords:
Piezoelectric
Dielectric
Ferroelectric
Phase transition
Thermal stability

ABSTRACT

The phase transition behavior and its effect on thermal stability of the piezoelectric properties of the $(1-x)[0.65PbMg_{1/3}Nb_{2/3}O_3–0.35PbTiO_3]–xBiZn_{1/2}Ti_{1/2}O_3$ ceramics with $0 \le x \le 0.06$ were investigated. The phase transition from the monoclinic to tetragonal phase was determined by the dielectric constant and elastic constant measurements. The temperature independent piezoelectric response with $-d_{31} = 188$ pC/N was obtained from 175 to 337 K for the composition with $x = 0.02$. The enhanced thermal stability of piezoelectric response was achieved by shifting the monoclinic–tetragonal phase transition to the lower temperature.

1. Introduction

Lead-based ferroelectric ceramics exhibit superior electromechanical properties at the morphotropic phase boundary (MPB) and have been widely used as actuators, sensors and transducers [1–3]. PMN–PT ceramics near the MPB show better piezoelectric properties than PZT [4]. These higher electromechanical properties originate from the enhanced extrinsic contribution not only from the lower Curie temperature (165 °C) but also from the ferroelectric–ferroelectric phase transition around 60–90 °C [5,6]. These low temperature phase transitions cause strong temperature dependence of the electromechanical properties, which limits their applications in wide temperature range [7].

Shifting the intermediate phase transformation to room temperature greatly improves the electromechanical activity in $BaTiO_3$ and (K,Na)NbO_3 piezoelectric ceramics, while the thermal stability of these ceramics has been sacrificed [8,9]. As known in dielectrics, increasing the diffuseness of the phase transformation could improve the thermal stability of dielectric properties [1].

Bismuth zinc titanate $Bi(Zn_{1/2}Ti_{1/2})O_3$ is a new lead free polar compound with the largest tetragonality ($c/a = 1.211$), the largest calculated point polar (150 μC/cm^2) ever reported in any d^0 B site Bi and Pb based perovskites, and high Curie temperature more than 900 °C [10]. Some interesting results have been reported in solid solutions of $Bi(Zn_{1/2}Ti_{1/2})O_3$ with other perovskites. The diffuseness of the phase transformation were enhanced after introducing $Bi(Zn_{1/2}Ti_{1/2})O_3$ into $PbTiO_3$, $BaTiO_3$ and $K_{1/2}Na_{1/2}NbO_3$ ceramics [11–13]. Especially, the intermediate phase transformation in $BaTiO_3$ and $K_{1/2}Na_{1/2}NbO_3$ have been tuning down to the lower temperature [12,13]. Although such notable and interesting effects have been observed, there are no reports of the BZT solid solution with high performance PMN–PT to our best knowledge.

High performance piezoelectric PMN–PT ceramics with MPB composition have been prevented from applications in the wide temperature range by their poor thermal stability of electromechanical properties. The aim of this work is to improve the thermal stability of piezoelectric response of PMN–PT ceramics by lowering and diffusing the intermediate ferroelectric–ferroelectric phase transformation with $Bi(Zn_{1/2}Ti_{1/2})O_3$. Therefore, the $(1-x)[0.65PbMg_{1/3}Nb_{2/3}O_3–0.35PbTiO_3]–xBiZn_{1/2}Ti_{1/2}O_3$ ceramics were prepared. The influences of $Bi(Zn_{1/2}Ti_{1/2})O_3$ on the crystal structure, phase transition behavior and electromechanical properties have been systematically investigated.

* Corresponding author. Tel.: +86 21 52412420; fax: +86 21 52413122.
** Corresponding author. Tel.: +852 34003345; fax: +852 23301544.
E-mail addresses: grli@mail.sic.ac.cn (G. Li), eeswor@polyu.edu.hk (S.W. Or).

0925-8388/$ – see front matter © 2011 Elsevier B.V. All rights reserved.
doi:10.1016/j.jallcom.2011.06.009

2. Experimental

The one-step solid reaction method was used to prepare compositions of $(1-x)[0.65PbMg_{1/3}Nb_{2/3}O_3–0.35PbTiO_3]–xBiZn_{1/2}Ti_{1/2}O_3$ (abbreviated as 0.65PMN–0.35PT–*x*BZT) where *x* in the range from 0 to 0.06. Pb_3O_4 (99.9%), Nb_2O_5 (99.9%), TiO_2 (99.9%), $4(MgCO_3)\cdot Mg(OH)_2\cdot 5H_2O$ (99.5%), Bi_2O_3 (99%), and ZnO (99.5%) were used as raw materials. These materials were weighed according to the designed composition. The raw materials were mixed for 24 h in deionized water. After drying, the powder was twice calcined at 1123 K for 4 h. Second ball milling was employed to reduce the powder size. The final powder was pressed into disks with the diameter of 12 mm and sintered in the temperature range of 1473–1523 K with the dwelling time of 0.5–2 h.

The density of the sample was measured by Archimedes method. The crystal structure was examined with XRD powder diffraction (scan rate 4°/min, step 0.02°, D/max-2550VX, Rigaku Corporation, Tokyo, Japan). The sample with silver electrodes was poled in the silicone oil at 335 K under a directive electric field of 3 kV/mm and then cooled down to room temperature under the electric filed. All electric measurements were conducted after aging at least for 48 h. The *P–E* hysteresis loops of samples were measured by a TF analyzer (Model 2000, aix ACCT Systems, Germany) at 20 °C. The temperature dependences of dielectric and piezoelectric properties were performed using an HP4294A precise impedance analyzer (Agilent Technologies Inc., Palo Alto, CA), according to IEEE standards [14]. The resonant f_r and antiresonant f_a frequencies are measured with an precision impedance analyzer. The elastic compliance constant s_{11}, the electromechanical coupling factors k_{31}, and the piezoelectric constant $-d_{31}$ are calculated according to the following equations provided in IEEE standards.

$$k_p = \left(\frac{f_a - f_r}{0.395f_r + 0.574(f_a - f_r)}\right)^{1/2} \quad (1)$$

In the case of $0.27 < \sigma^E < 0.42$, the Poisson ratio can be calculated by equation

$$\sigma^E = \frac{5.332f_r - 1.867f_{r,1}}{0.6054f_{r,1} - 0.1910f_r} \quad (2)$$

$$k_{31} = k_p\sqrt{\frac{1-\sigma^E}{2}} \quad (3)$$

$$s_{11}^E = \frac{\eta_1^2}{(\pi\cdot d\cdot f_r)^2\cdot(1-\sigma^{E2})\cdot\rho} \quad (4)$$

$$d_{31} = -k_{31}\sqrt{\varepsilon_{33}^T\cdot s_{11}^E} \quad (5)$$

where f_r is the resonance frequency, f_a the anti-resonance frequency, $f_{r,1}$ the first overtone frequency, σ^E the Poisson ratio, and ρ the density of the investigated sample, d the diameter of sample, η_1 the minimal root of the equation: $(1+\sigma^E)J(\eta) = \eta J_0(\eta)$. The sample temperature was controlled by a liquid nitrogen bath cryostat (DN-1704, Oxford Instrument, UK), stabilized by a digital temperature controller (ITC 601, Oxford Instrument, UK).

3. Results and discussion

The crystal structure of the 0.65PMN–0.35PT–*x*BZT ceramics before poling was examined by XRD, as shown in Fig. 1a. All compositions show pure perovskite phases with tetragonal structure. No secondary phase could be found after the addition of BZT. As Bi^{3+} (1.34 Å) is smaller than Pb (1.49 Å) while Zn (0.74 Å) are similar with Mg (0.72 Å) [15]. The diffraction lines slightly shifts towards the higher angle, as seen in Fig. 1b. A continuously broadening of diffraction lines has been observed with *x* increasing from 0 to 0.06. This broadening indicates the increase of internal strain from compositional disorder. The local tetragonal distortion randomly distributes in ceramics, resulting in the broadened diffraction lines [16]. Theoretical *ab initio* calculation revealed that hybridization of the Zn 4s, 4p and O 2p orbitals form the short covalent Zn–O bonds in BZT–PT [17]. These short bonds increase the off-center displacement of A-site and B-site ions in the perovskite structure and increase the tetragonal distortion. This result is consistent with our experimental XRD observation.

Fig. 2 shows the SEM results of the fracture of 0.65PMN–0.35PT–*x*BZT ceramics. The grain sizes of 0.65PMN–0.35PT ceramic range from 5 to 9 μm and small amount of pores are observed. The clean grain boundary indicates the intergranular fracture. After solidification between 0.65PMN–0.35PT and BZT ($x = 0.04$, 0.06), the ceramics became denser. It should be addressed that notable transgranular fracture has been induced. One possible reason is that the internal strain caused by replacement of Bi for Pb decreases the strength of the grain [18]. This result is supported by the XRD results.

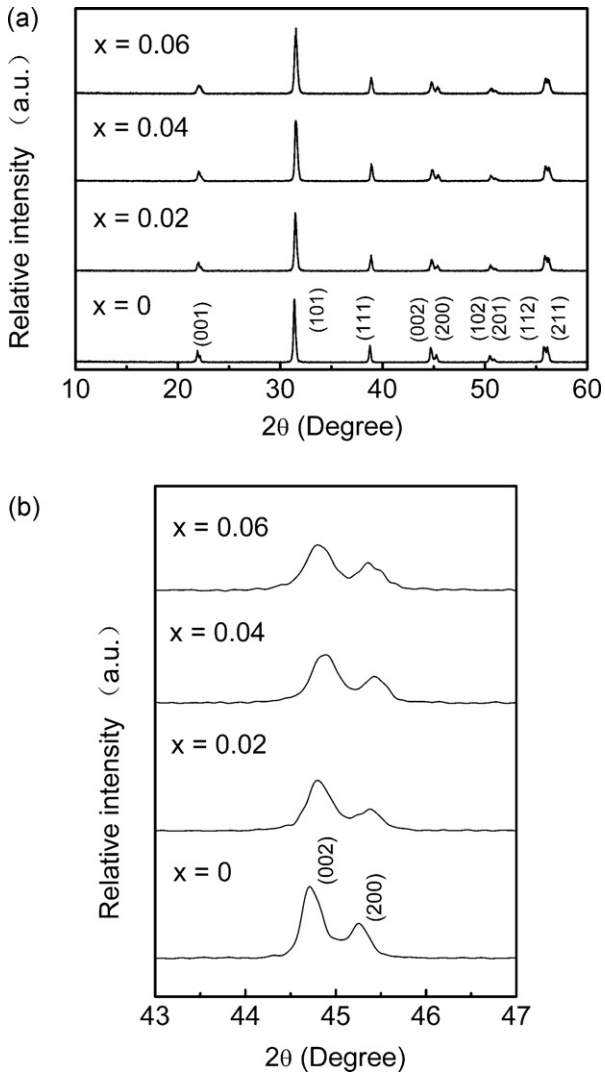

Fig. 1. The XRD patterns of 0.65PMN–0.35PT–*x*BZT ceramics with 2θ in the range from (a) 15° to 80° and (b) 43° to 47°.

Fig. 3 shows the variations of dielectric constant (ε_r) with composition and temperature at 1 kHz for poled 0.65PMN–0.35PT–*x*BZT ceramics during heating from 77 to 500 K. To clearly demonstrate the low temperature phase transition, the reciprocal of the dielectric constant ($1/\varepsilon_r$) are also showed. For the pure 0.65PMN–0.35PT, a sharp dielectric anomaly is observed at 442 K, corresponding to cubic to tetragonal phase transition. Another dielectric anomaly at 332 K should be related to an electric field induced phase transition [5,6]. The increase of *x* increases the diffuseness and lowers phase transformation temperatures of these phase transitions. The increase of the diffuseness by doping is generally observed in relaxor ferroelectrics and can be attributed to the compositional and/or structural disorder in the ceramics or crystals [19]. The partial substitution of Bi for Pb on the A site and Zn for Ti on B site increase the local compositional disorder, enhancing the diffuse character of the phase transition, which is similar to that in BZT doped $BaTiO_3$ [12]. The replacement of the smaller ion Bi for Pb results in local tense stress, which could enhance the mobility of A ion and decreases the phase transition temperature.

As demonstrated in the piezoelectric ceramics, the ferroelectric–ferroelectric phase transition around the room

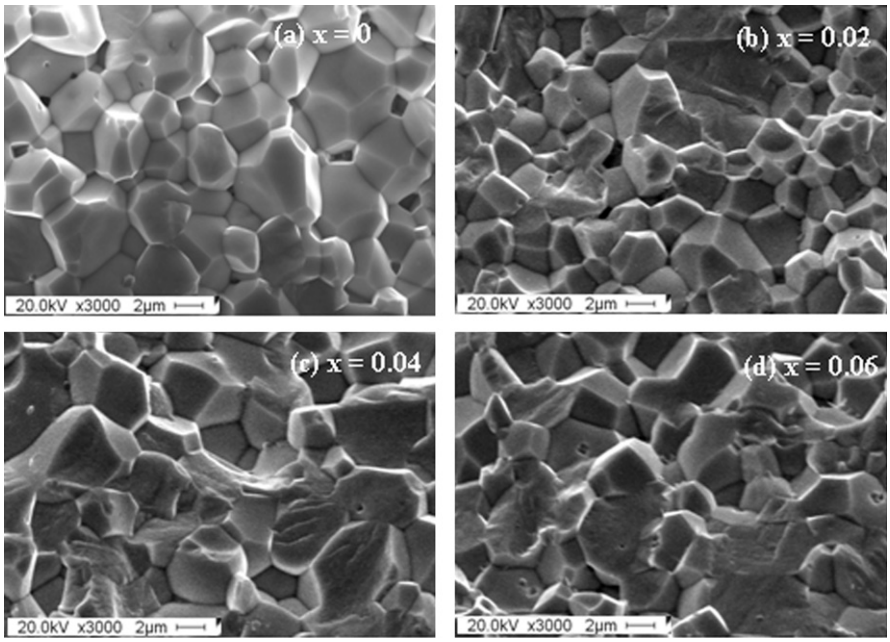

Fig. 2. SEM results of 0.65PMN–0.35PT–*x*BZT: (a) $x = 0$, (b) $x = 0.02$, (c) $x = 0.04$, and (d) $x = 0.06$.

temperature strongly affects the electromechanical properties and their temperature stability [20,21]. To monitor the low temperature phase transition, the temperature and composition dependences of elastic compliance constant are investigated from 77 to 337 K in Fig. 4. Around a phase transition, the softening of the crystal lattice as the temperature changes will result in an elastic peak [22,23]. The diffuse elastic peaks in Fig. 4 signify the low temperature phase transition in the PMN–PT ceramics. A low temperature phase to the tetragonal phase transition caused the low temperature dielectric anomaly in PMN–PT crystal [24]. Although this low temperature phase transformation has been suggested as the rhombohedral (R)–tetragonal (T) phase transition [25]. Noheda et al. [26] showed that the $(1-x)$PMN–xPT ceramic with $x = 0.35$ would undergo monoclinic (M) to tetragonal (T) and tetragonal (T) to cubic (C) phase transition as the temperature increases. Therefore, this low temperature phase transition might correspond to the M–T phase transition. As seen from Figs. 4 and 3, the M–T phase transition has been shifted below room temperature with increasing BZT. But the diffuseness of these elastic peaks makes it difficult to determine the exact temperature of the phase transition. However, discrete kinks at the low temperature, corresponding to the M–T phase transition, have been clearly observed from the temperature dependence of dielectric constant (Fig. 3). These diffusive dielectric anomalies effectively improve the low temperature dielectric constant and decrease its temperature dependence. The temperatures of low temperature phase transitions (T_{M-T}) could be roughly identi-

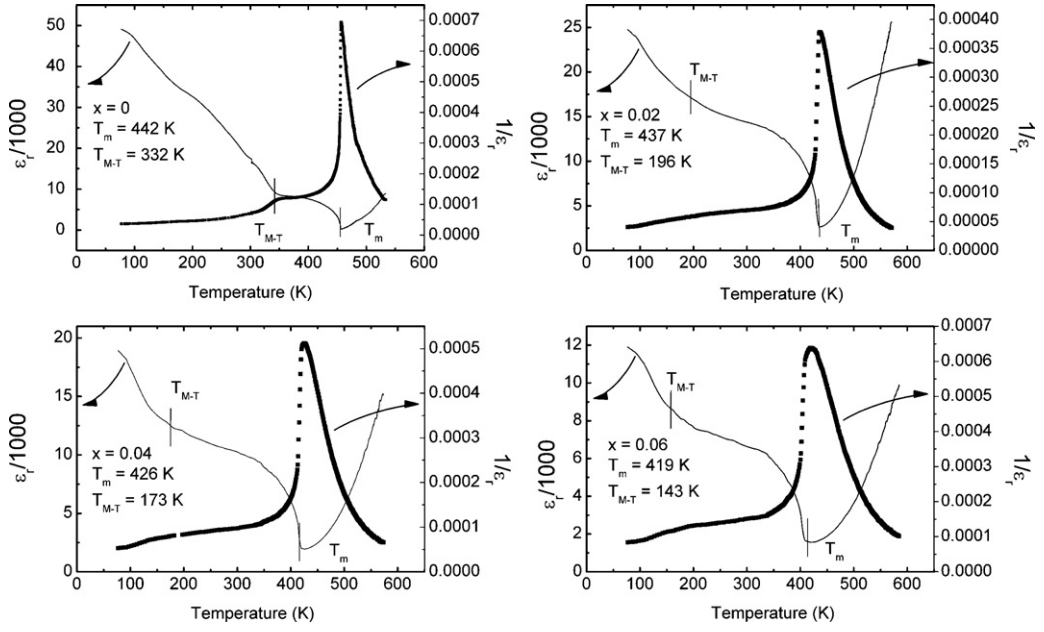

Fig. 3. The relative dielectric constant and its reciprocal of 0.65PMN–0.35PT–*x*BZT ceramics as functions of temperature and BZT concentration.

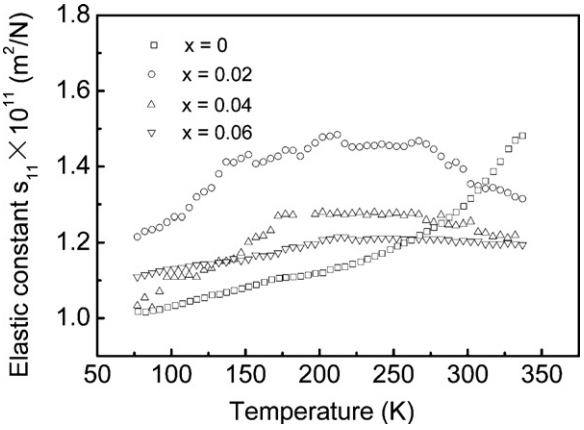

Fig. 4. The temperature and composition dependence of elastic compliance constant s_{11} of 0.65PMN–0.35PT–*x*BZT ceramics in the low temperature.

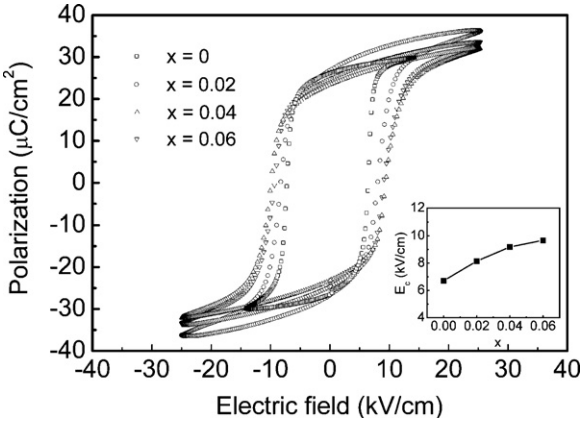

Fig. 6. The *P*–*E* loops of 0.65PMN–0.35PT–*x*BZT ceramics with $0 \le x \le 0.06$.

fied from those kinks of the reciprocal of dielectric constant in Fig. 3.

The phase transition temperature corresponding to that of the maximum dielectric constant is abbreviated as T_m. T_m as obtained from temperature dependences of dielectric constant is reported in Fig. 5. T_m nearly decreases linearly with the increase of *x* at the rate of about 3.6 K/0.01 mol. However, the T_{M-T} initially decreases at the rate of about 64 K/0.01 mol when $x \le 0.02$, then decreases at the rate of about 10 K/0.01. The pseudo phase diagram of 0.65PMN–0.35PT–*x*BZT ceramics after poling could be constructed based on the phase transition temperatures T_m and T_{M-T}. The larger decrease in T_{M-T} than that in T_m greatly extends the tetragonal phase region. It should be stressed that 0.65PMN–0.35PT ceramic has transformed to monoclinic phase after poling. Similar electric field induced phase transition has been reported [27].

Fig. 6 shows the *P*–*E* loops of the 0.65PMN–0.35PT–*x*BZT ceramics with *x* = 0, 0.02, 0.04, and 0.06. All the ceramics exhibit a well-saturated *P*–*E* loop under an electric field of 10–25 kV/cm. The pure 0.65PMN–0.35PT ceramic shows a square *P*–*E* loop with large remnant polarization P_r (26.14 μC/cm²) and low coercive electric field (6.17 kV/cm). After addition of BZT, the remnant polarization P_r shows a slight change while the coercive electric field monotonously increases. The microstructure observation (Fig. 2) shows that the grain size of the 0.65PMN–0.35PT–*x*BZT ceramics has a diameter in the range of 5–9 μm and does not distinctly decrease with the increase of BZT. This observation suggests that the increase of the E_c is not due to the clamping effect of the small grain [28]. As known, the domain wall motion is highly active near MPB, which causes the lower coercive electric field [1]. Temperature induced phase transformation should play similar role in the change of coercive electric field. As increasing of *x*, the low temperature M–T phase transformation sharply deviate from room temperature, which obviously extends the stable region of tetragonal phase as seen in Fig. 5.

Fig. 7 shows the temperature dependence of piezoelectric constant $-d_{31}$ in the range from 77 to 337 K. For the pure 0.65PMN–0.35PT ceramic, the piezoelectric constant $-d_{31}$ is higher than that of the compositions with the BZT addition in the temperature range III (277–337). However, it greatly decreases from 285 to 182 pC/N when the temperature decreases from 337 to 277 K. The strong temperature dependence of piezoelectric constant limits its applications in the wide temperature range. This high electromechanical properties and strong temperature dependency should originate from the ferroelectric monoclinic to tetragonal phase transition around 332 K as shown in Fig. 3. Since the domain wall motion is highly active near the phase transition. Similar result has been reported in the lead free ceramics [29]. The pure 0.65PMN–0.35PT ceramic undergoes a monoclinic to tetragonal (M–T) phase transition near room temperature, which results in a low coercive electric field (6.17 kV/cm) and high domain wall activity. During decreasing temperature, the decrease of the domain wall motion induces the strong temperature dependence of piezoelectric response in temperature range II and III. At *x* = 0.02, the M–T phase transition has been sharply shifted down to 196 K. The piezoelectric response in temperature III decreases as departing from

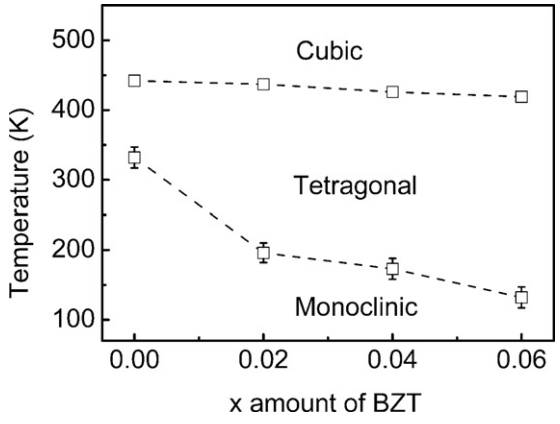

Fig. 5. The pseudo phase diagram of 0.65PMN–0.35PT–*x*BZT ceramics with $0 \le x \le 0.06$ after poling.

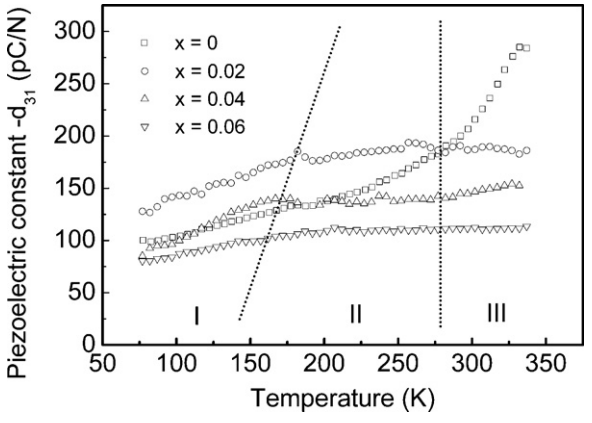

Fig. 7. The temperature and composition dependence of piezoelectric coefficient $-d_{31}$ of 0.65PMN–0.35PT–*x*BZT ceramics.

the M–T phase transition, while the electromechanical properties in range of II (175–277) increases by the M–T phase transition and become higher than that of pure 0.65PMN–0.35PT. A well-resolved piezoelectric plateau with $-d_{31}$ about 180 pC/N is observed from 175 to 337 K. With further increasing BZT, the deviations from the M–T phase transitions in Fig. 7 increase the coercive electric field, which suppress the domain wall motion and decrease its temperature dependence. Therefore, the piezoelectric constant plateau still could be observed but its value decreases to 135 and 110 pC/N for compositions with $x = 0.04$ and 0.06, respectively. Further deviation from the low temperature M–T phase transition, the piezoelectric constants of all compositions decrease below 170 K.

4. Conclusions

0.65PMN–0.35PT–xBZT piezoelectric ceramics have been fabricated by the solid state reaction method. A low temperature M–T phase transition has been revealed by dielectric and elastic measurements. The diffuseness of M–T phase transition increases with increasing BZT content. The temperatures of T–C phase transition and M–T phase transition decrease with increasing BZT content. Through tuning down the M–T phase transition to low temperature, the thermal stability of piezoelectric properties could be enhanced. The temperature independent piezoelectric response with $-d_{31} = 188$ pC/N ($d_{33} = 450$ pC/N) was obtained from 175 to 337 K for the composition with $x = 0.02$, which make it a promising candidate for wide temperature application.

Acknowledgements

This work was supported by the Ministry of Sciences and Technology of China through 973-project (No. 2009CB623305), Natural Science Foundation of China (No. 50675218), the Research Grants Council of the HKSAR Government (No. PolyU 5266/08E), The Hong Kong Polytechnic University (Nos. 1-ZV7P and G-U741), and the key project of Inner Mongolia University of Technology (ZD200314).

References

[1] B. Jaffe, W.R. Cook, H. Jaffe, Piezoelectric Ceramics, Academic Press, New York, 1971.
[2] G.H. Haertling, J. Am. Ceram. Soc. 82 (1999) 797.
[3] K. Uchino, Ferroelectric Devices, Marcel Dekker Inc., New York, 2000.
[4] J. Kelly, M. Leinard, C. Tantigate, A. Safari, J. Am. Ceram. Soc. 80 (1997) 957.
[5] S.-E. Park, T.R. Shrout, J. Appl. Phys. 82 (1997) 1804.
[6] Z. Cao, G. Li, J. Zeng, L. Zheng, Q. Yin, J. Phys. D: Appl. Phys. 43 (2010) 015405.
[7] P.C. Wang, X.M. Pan, D.L. Li, Y.W. Song, H.S. Luo, Z.W. Yin, J. Mater. Res. 18 (2003) 537.
[8] Y. Avrahami, H.L. Tuller, J. Electroceram. 13 (2004) 463.
[9] Y. Guo, K. Kakimoto, H. Ohsato, Appl. Phys. Lett. 85 (2004) 4121.
[10] M.R. Suchomel, A.M. Fogg, M. Allix, H. Niu, J.B. Claridge, M.J. Rosseinsky, Chem. Mater. 18 (2006) 4987.
[11] M.R. Suchomel, P.K. Davies, Appl. Phys. Lett. 86 (2005) 262905.
[12] C.-C. Huang, D.P. Cann, J. Appl. Phys. 104 (2008) 024117.
[13] M. Sutapun, C.C. Huang, D.P. Cann, N. Vittayakorn, J. Alloys Compd. 479 (2009) 462.
[14] IEEE Standard on Piezoelectricity, IEEE, New York, 1987.
[15] R.D. Shannon, Acta Crystallogr. A32 (1976) 751.
[16] X. Dai, Z. Xu, D. Viehland, J. Appl. Phys. 79 (1996) 1021.
[17] I. Grinberg, M.R. Suchomel, W. Dmowski, S.E. Mason, H. Wu, P.K. Davies, A.M. Rappe, Phys. Rev. Lett. 98 (2007) 107601.
[18] Z.Q. Zhuang, M.J. Haun, S.J. Jiang, L.E. Cross, Applications of Ferroelectrics. 1986 Sixth IEEE International Symposium on IEEE, 1986, p. 394.
[19] L.E. Cross, Ferroelectrics 76 (1987) 241.
[20] T.R. Shrout, S.J. Zhang, J. Electroceram. 19 (2007) 113.
[21] J. Wu, D. Xiao, Y. Wang, W. Wu, B. Zhang, J. Li, J. Zhu, Scr. Mater. 59 (2008) 750.
[22] M. Rosen, Phys. Rev. 181 (1969) 932.
[23] B. Jiménez, J.M. Vicente, J. Phys. D: Appl. Phys. 31 (1998) 130.
[24] A. Sehirlioglu, D.A. Payne, P. Han, J. Appl. Phys. 99 (2006) 064101.
[25] S. Park, T.R. Shrout, J. Appl. Phys. 82 (1997) 1804.
[26] B. Noheda, D.E. Cox, G. Shirane, J. Gao, Z.-G. Ye, Phys. Rev. B 66 (2002) 054104.
[27] K.P. Chen, X.W. Zhang, H.S. Luo, J. Phys.: Condens. Matter 14 (2002) L571.
[28] D. Damjanovic, M. Demartin, J. Phys.: Condens. Matter 9 (1997) 4943.
[29] Z. Feng, S.W. Or, J. Alloys Compd. 480 (2009) L5.